Q. Xie, S. Afshar, A. Ozgurluk, and C. T.-C. Nguyen, "199-MHz polysilicon micromechanical disk array-composite oscillator," *Proceedings*, IEEE Joint Conf. of the IEEE Int. Frequency Contr. Symp. & IEEE Int. Symp. on Applications of Ferroelectrics, Virtual Conference, July 19-23, 2020, DOI: 10.1109/IFCS-ISAF41089.2020.9234862. ***(best paper award winner)***

199-MHz Polysilicon Micromechanical Disk Array-Composite Oscillator

Qianyi Xie, Sherwin Afshar, Alper Ozgurluk, and Clark T.-C. Nguyen

Berkeley Sensor & Actuator Center (BSAC)
Dept. of Electrical Engineering and Computer Sciences
University of California at Berkeley
Berkeley, California, USA
qianyi_xie@berkeley.edu

***Abstract*—The use of a stress-buffered array-composite of six 13.4-µm radius capacitive-gap transduced radial-contour mode polysilicon micromechanical disk resonators with 36.1-nm electrode-to-resonator gaps has enabled a Pierce oscillator centered at 199.2 MHz with phase noise marks of -104.7dBc/Hz at 1-kHz offset and -149.6dBc/Hz far from the carrier, sufficient for smartphones. The 12-kHz to 20-MHz integrated jitter is 163.3fs, which yields an excellent jitter FoM of –251dB. The key to this demonstration is the use of λ couplers to affect a 0^0 phase shift across the array terminals; and electrodeless resonators to buffer the effect of post-fabrication stress that otherwise might short disks to their electrodes when gaps are very small.**

***Keywords*—MEMS, stress buffer, quality factor, VHF, resonator, array, Pierce.**

I. Introduction

The high Q of capacitive-gap transduced micromechanical resonators has recently permitted best-in-class oscillator figure of merit (FOM), with the 61-MHz implementation of [1] achieving -119 dBc/Hz at 1-kHz offset and -139 dBc/Hz far from the carrier while consuming only 78 µW. These marks make this oscillator suitable for use as a reference for communication synthesizers, especially those targeted for very low power applications, e.g., set-and-forget autonomous sensor networks. While use of the oscillator in [1] does save power, its conventional oscillation frequency does little to reduce the power consumed by a synthesizer's VCO, phase-detector, and frequency divider [2], which often dominate power consumption. To reduce their power draw, a higher frequency oscillator that preserves good phase noise performance is in order.

Pursuant to reducing the requirements, and hence power consumption, of the phase detector and frequency divider circuits in a synthesizer, this work employs gap-scaling, beam-coupled arraying, and strategic stress-relieving buffers to achieve a coupled mechanical circuit that permits a rise in reference oscillator frequency to 199.2 MHz while still retaining phase noise performance commensurate with smart phone requirements.

II. Disk Array-Composite Resonator and Oscillator Circuit

Fig. 1 presents (a) the oscillator circuit with (b) the perspective-view schematic of the disk array-composite resonator that

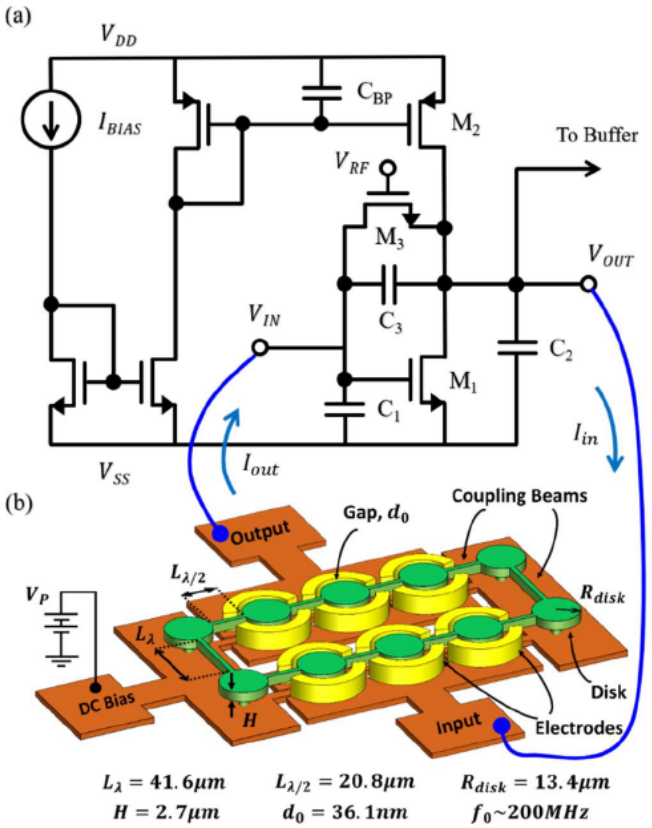

Fig. 1: (a) Oscillator circuit and (b) perspective-view illustration of its 5-disk array-composite resonator frequency-setting element.

enables 199.2-MHz operation. Here, a similar Pierce-based circuit to that of [1] serves as the sustaining amplifier with C_1 and C_2 values chosen to insure oscillation startup at 199.2 MHz. Fig. 2 presents a plot of the negative resistance R_{amp} (described in [1]) generated by the amplifier versus transistor M_1 transconductance g_m, showing how a very small C_3 and correct choice of capacitors insures sufficient gain even for a motional resistance R_x as high as 3.3 kΩ. The disk array-composite resonator in Fig. 1(b) comprises two 5-disk half-wavelength beam coupled arrays, themselves coupled by full-wavelength beams between electrodeless disks. Here, half-wavelength coupling forces all resonators in an array-composite to resonate in phase, allowing summation of their outputs towards a smaller R_x. The

978-1-7281-6430-4/20/$31.00 ©2020 IEEE

full-wavelength coupling beams force the input and output arrays to vibrate 180° out-of-phase, which then provides the 0° phase shift across the resonator array-composite I/O terminals needed for oscillation [1].

The use of arrays, together with 36.1-nm electrode-to-resonator gaps (down from the 80-nm of [1]), enables a reasonable R_x of 3.3 kΩ despite the 3.3 times higher frequency than [1] and ultimately enables oscillator operation at 199.2 MHz. Perhaps more important, however, is the use of electrodeless buffer disks at the ends of the arrays [3]. These move with post-fabrication stress to alleviate strain in the inner electrode-equipped resonators, preventing them from pushing into their electrodes.

III. Mechanically Coupled Array-Composite Resonator

To explain the need to mechanically couple resonators rather than use an uncoupled array of individual, identically drawn resonators, Fig. 3 summarizes the basic issues using a plot of output current versus input voltage for three cases: (a) a single disk resonator; (b) an array of uncoupled disks; (c) a coupled array, i.e. array-composite, of electrode-equipped disk resonators; and (d) a coupled array with electrodeless buffer disks at its ends. Here, the goal of arraying N resonators is to sum electrode-equipped resonator currents so that the total output current is N times larger than that of a single resonator for the same input voltage, which then means the motional resistance $R_x = v_i/i_x$ gets smaller by N times.

Note how the extremely high Q of its constituent disk resonators essentially precludes the uncoupled resonator array (case (b)) from summing currents. Instead, its output comprises several individual resonator current peaks that do not combine because for real devices their frequencies are not precisely the same—a consequence of finite fabrication tolerances. If the Q's of the resonators were substantially lower, then their peaks would be broad enough to traverse the range of frequencies, allowing currents to add appreciably. However, for an application that requires high Q, e.g., the present oscillator application, use of an uncoupled resonator array will not work.

As illustrated in Fig. 3(c), coupling solves this problem by forcing all resonators to vibrate in one resonance mode, i.e., at one frequency. The resulting coupled resonator system has many modes, at least as many as the number of resonators in the array. However, the use of half-wavelength coupling beams and strategic phasing of voltages applied to the electrodes help to isolate a specific mode and push other modes further away [4]. The result: An array of high Q resonators that effectively behaves like a composite resonator outputting N times more current at its isolated resonance frequency for a given input voltage, hence attaining an N times smaller motional resistance.

As described in past literature [5], one additional benefit of mechanical coupled arraying is better stability against biasing and impedance changes brought about by both long- (e.g., aging) and short-term (e.g., supply noise) deviations. This manifests from the negative capacitance inherent in the equivalent circuit model for parallel-plate capacitive-gap transduced resonators [6].

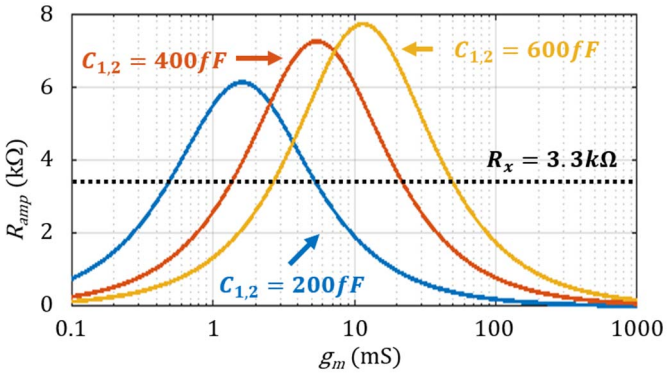

Fig. 2: Impact of $C_{1,2}$ on the achievable amplifier negative impedance (R_{Amp}) with C_3=45fF at 199.2MHz. Here, small C_3 allows $C_{1,2}$'s as small as small as 200fF to startup oscillation for a resonator motional resistance of 3.3kΩ.

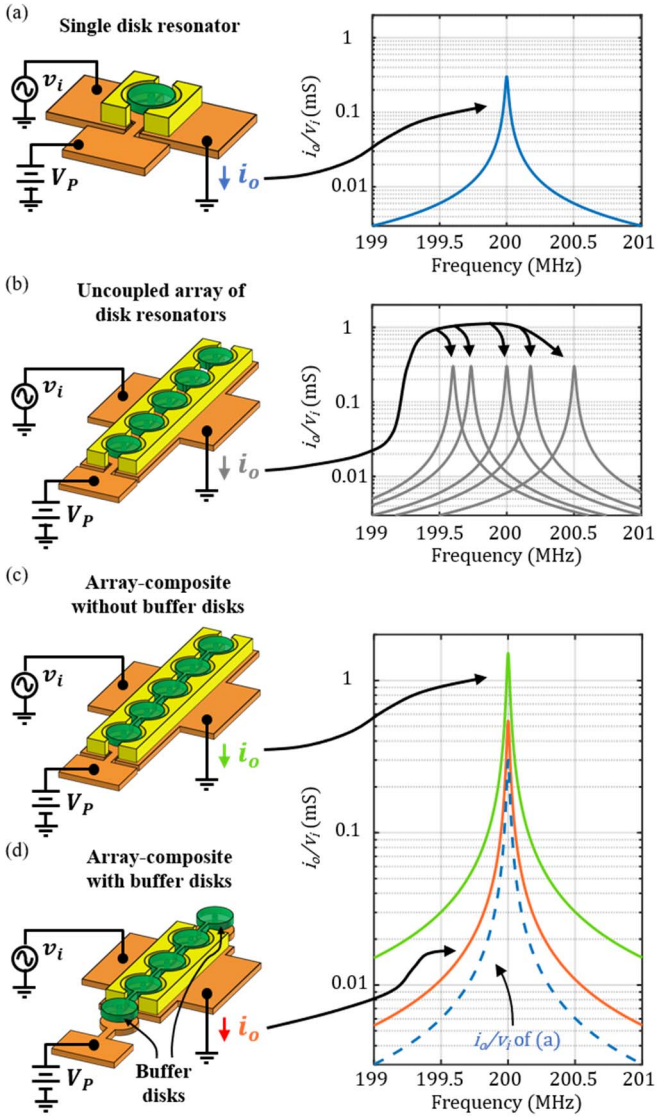

Fig. 3: Voltage-to-current (i_o/v_i) frequency responses of (a) a single disk having a single peak, (b) an uncoupled disk array-composite resonator having 5 separate peaks due to mismatch, (c) a λ /2-coupled disk array-composite resonator having a single stronger peak, and (d) a λ/2-coupled disk array-composite resonator with electrodeless buffer disks that weaken the output current versus a that of a full-electrode array-composite resonator but remains stronger than the single disk resonator peak.

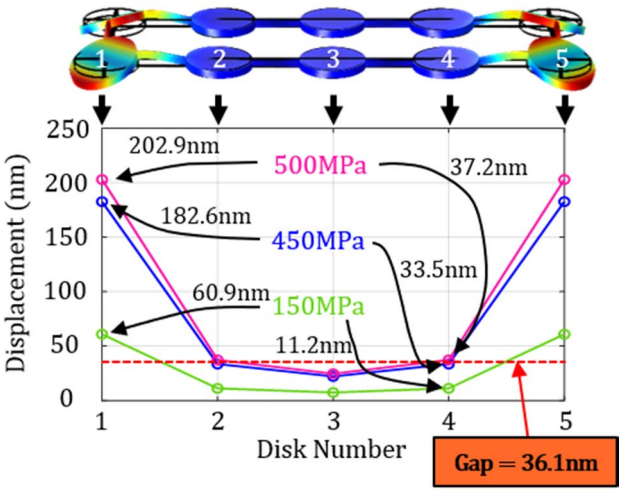

Fig. 4: After-release displacement of each disk in the array-composite under various values of compressive stress. The introduction of buffer disks reduces the displacement of inner disks and ensure they do not touch electrodes.

IV. Stress Buffer Disks

Unfortunately, mechanical coupling of disks increases susceptibility to stress, especially as electrode-to-resonator gaps get smaller. Specifically, one failure mode to avoid occurs when stress pushes a disk into its electrode. For the present work, a disk need only traverse a 36.1-nm gap before it touches its electrode. This problem will get worse as gaps shrink for future devices attempting to attain even higher frequency.

Fortunately, there is a simple design solution: Remove electrodes from the disks at the ends of each linear array, which converts the array from that of Fig. 3(c) into that Fig. 3(d), which in turn is the same as either the top or bottom linear array of Fig. 1. Fig. 4 captures the efficacy of this approach by plotting the finite-element-simulated lateral displacement of each disk in a 5-disk array as a function of stress. Note how the end resonators absorb most of the stress and move the most, allowing the inner resonators to move very little. Using this stress buffer strategy, it would take more than 450 MPa of residual stress to push inner disks with the 36.1-nm gaps used here into their electrodes. This is considerably more residual stress than the 150 MPa typical of polysilicon surface micromachining processes.

While effective in solving stress issues, the use of buffer disks does impose a reduction in the overall effective electromechanical coupling of a resonator array, and hence an increase in motional resistance. This comes about because buffer disks increase the overall stiffness of the array-composite without contributing to electromechanical coupling (since they are electrodeless). As a consequence, the motional resistance for a *N*-disk array-composite using *M* electrodeless buffer disks takes the form [7]:

$$R_{x,N,M} = \frac{c_{re,N,M}}{\eta_{N,M}^2} = \frac{N \cdot c_{re,0}}{[(N-M)\cdot\eta_0]^2} = \frac{N}{(N-M)^2} \cdot R_{x,0} \qquad (1)$$

$$R_{x,N,N} = \frac{N}{N^2} \cdot R_{x,0} = \frac{1}{N} \cdot R_{x,0} \qquad (2)$$

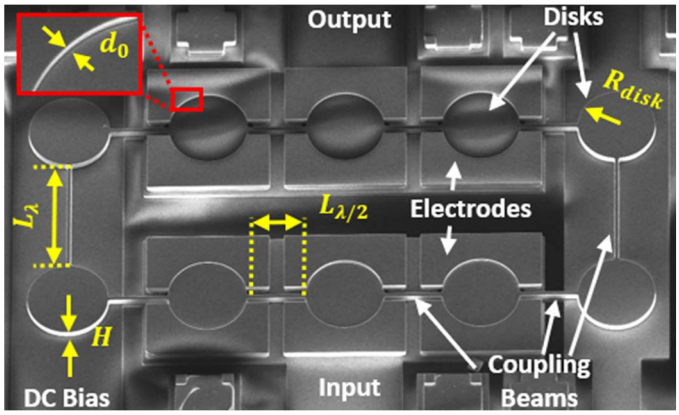

Fig. 5: Scanning electron micrograph (SEM) image of the 199.2-MHz polysilicon disk array-composite resonator.

where $R_{x,N,M}$, $c_{re.N,M}$ and $\eta_{N,M}$ are the motional resistance, mechanical damping factor and electro-mechanical coupling factor of the *N*-disk array-composite using *M* electrodeless buffer disks, $R_{x,0}$, $c_{re.0}$ and η_0 are the motional resistance, mechanical damping factor and electro-mechanical coupling factor of a single disk resonator, and $R_{x,N,N}$ is the motional resistance of a *N*-disk array-composite where all disks have electrodes.

Equation (1) and (2) indicate a motional resistance $\left(\frac{N}{N-M}\right)^2$ times larger for an *N*-disk, *M*-electrode array-composite than for an *N*-disk array-composite where all disks have electrodes. For the design of this work, R_x goes from 1.2 kΩ to 3.3 kΩ upon (the necessary) introduction of buffer disks. 3.3 kΩ is still smaller than the 7.9 kΩ worst case R_{amp} shown in Fig. 2 for the Pierce sustaining circuit of Fig. 1 at 200 MHz, so oscillation should still ensue.

V. Measurement Results

Fig. 5 presents the SEM of a fabricated polysilicon disk array-composite using the topology and dimensions summarized in Fig. 1(b). The fabrication used the tiny-gap surface micromachining process of [8] that yields the cross-section of Fig. 6 where the main difference from previous such processes is a much thicker 2.5-µm-thick interconnect doped polysilicon that reduces interconnect sheet resistance down to 2.7Ω/□ (from the previous 20.6 Ω/□ for 400-nm-thick interconnect [9]). This helps to prevent undue *Q*-loading, which becomes more important as gap-shrinking and arraying reduce resonator motional resistance [8].

Fig. 7(a) presents a photo of the oscillator test apparatus, where the bond-wired resonator and custom-IC dies reside on a package that itself mounts on a pc-board placed inside a vacuum bulb. Before bond-wiring, measurement of the disk-array composite under 5 mTorr vacuum using probes in a vacuum probe station yields a *Q* of 19,921 at 199.2-MHz, as shown in Fig. 7(b). This *Q* is key to the performance of the oscillator.

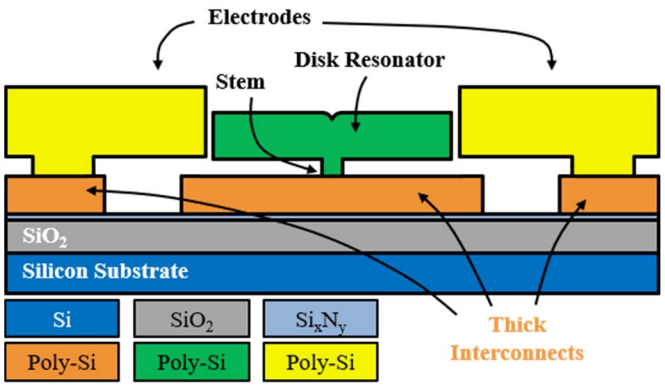

Fig. 6: Cross-section view of a released single disk resonator.

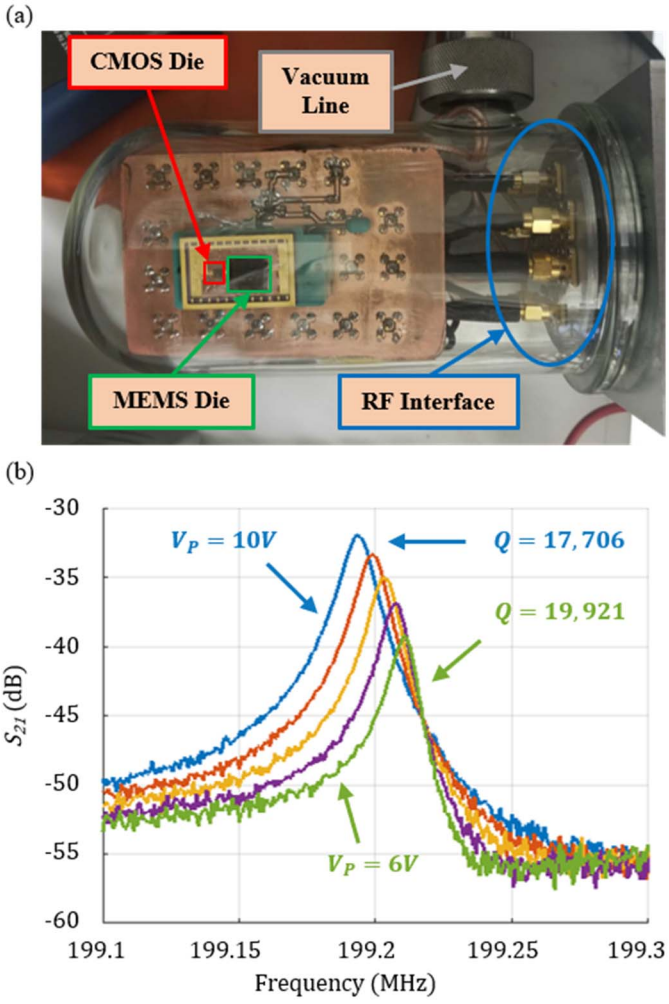

Fig. 7: (a) The test apparatus, and (b) measured S_{21} plots of the 199.2-MHz polysilicon disk array-composite with V_P of 6V, 7V, 8V, 9V and 10V.

It should be noted that disk array-composites without the electrodeless buffer disks were non-functional, emphasizing the importance of the buffers in resonator array design. In addition, there is evidence that bond-wiring reduces the Q of the disk resonator, sometimes down to one-half, perhaps due to ESD or ultrasonic-induced damage. Correct bond-wire recipe alleviates this to some degree, but a best recipe was yet to be found at the time of measurement. As a result, it is presently unclear whether

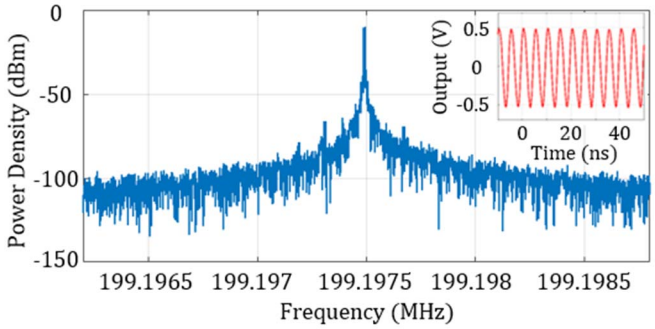

Fig. 8: Output power spectrum of the 199.2MHz oscillator. Inset: the measured output waveform.

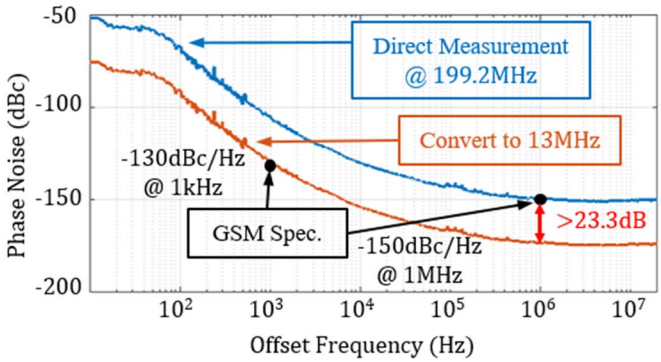

Fig. 9: Direct phase noise measurement of the 199.2MHz oscillator (Blue) and the phase noise after down-conversion to 13MHz (Orange).

the (bond-wired) disk array-composite used for oscillator demonstration truly had a Q near 20,000.

Nevertheless, judging from the measured oscillator performance its Q still must have been quite good. Fig. 8 presents the measured oscilloscope waveform and spectrum analyzer frequency output of the oscillator, showing an oscillation amplitude of $1V_{p\text{-}p}$, which is larger than that of the 61-MHz single-disk of $600mV_{p\text{-}p}$ [1], likely due to the higher linearity of the disk array-composite. This larger output swing contributes to better phase noise performance, as shown in Fig. 9 which presents the direct measured phase noise of the 199.2-MHz oscillator, as well as that seen when dividing down to 13 MHz for comparison with GSM specs. Here, the far-from-carrier phase noise of -173.3 dBc/Hz at 13 MHz easily satisfies the GSM requirement, while the phase noise at 1-kHz of -128.4 dBc/Hz is very close to the -130 dBc/Hz GSM specification. The 12-kHz to 20-MHz integrated phase jitter of the oscillator is 163.3fs, with a jitter figure of merit (FoM) of -251dB, which is quite good [10] [11] [12].

VI. Conclusions

The phase jitter of 163.3fs at 199.2 MHz demonstrated here derives from both the good close-to-carrier phase noise (enabled by a Q of 19,921) and low far-from-carrier phase noise. With even smaller gaps, such as demonstrated in [8] [13], the voltage-controlled tuning range of capacitive-gap transduced resonator oscillators like this might eventually become large enough to realize a synthesizer using an array of tunable oscillators, obviating the need for phase-lock loop circuits and opening a

path towards sizable advances in phase noise performance. Work towards such a synthesizer is ongoing.

ACKNOWLEDGMENT

The authors are grateful for funding support from NSF and the Berkeley Sensor &Actuator Center.

REFERENCES

[1] T. L. Naing, T. O. Rocheleau, E. Alon and C. T.-C. Nguyen, "A 78-Microwatt GSM Phase Noise-Compliant Pierce Oscillator Referenced to a 61-MHz Wine-Glass Disk Resonator," *IEEE Transactions on Ultrasonics, Ferroelectrics, and Frequency Control,* vol. 67, no. 7, pp. 1377-1391, July 2020, DOI: 10.1109/TUFFC.2020.2969530.

[2] Silicon Labs, "Ultra Series Crysttal Oscillator Si545 Data Sheet," July 2018. [Online]. Available: https://www.silabs.com/documents/public/data-sheets/si545-datasheet.pdf. [Accessed 21 February 2020].

[3] M. Akgul, A. Ozgurluk and C. T.-C. Nguyen, "RF Channel-Select Micromechanical Disk Filters, Part II: Demonstration," *IEEE Transactions on Ultrasonics, Ferroelectrics, and Frequency Control,* vol. 66, no. 1, pp. 218-235, Jan. 2019, DOI: 10.1109/TUFFC.2018.2883296.

[4] Y.-W. Lin, S.-S. Li, Z. Ren and C. Nguyen, "Low phase noise array-composite micromechanical wine-glass disk oscillator," in *IEEE InternationalElectron Devices Meeting, 2005.*, Washington, DC, USA, Dec. 2005, pp. 287-290.

[5] L. Wu, M. Akgul, W.-C. Li, Z. Ren, T. Rocheleau and C. T.-C. Nguyen, "Micromechanical disk array for enhanced frequency stability against bias voltage fluctuations," in *2013 Joint European Frequency and Time Forum & International Frequency Control Symposium (EFTF/IFC)*, Prague, Czech Republic, July 2013, pp. 547-550.

[6] M. Akgul, L. Wu, Z. Ren and C. T.-C. Nguyen, "A negative-capacitance equivalent circuit model for parallel-plate capacitive-gap-transduced micromechanical resonators," *IEEE Transactions on Ultrasonics, Ferroelectrics, and Frequency Control,* vol. 61, no. 5, pp. 849-869, May 2014, DOI: 10.1109/TUFFC.2014.2976.

[7] A. Ozgurluk, M. Akgul and C. T.-C. Nguyen, "RF Channel-Select Micromechanical Disk Filters—Part I: Design," *IEEE Transactions on Ultrasonics, Ferroelectrics, and Frequency Control,* vol. 66, no. 1, pp. 192-217, Jan. 2019, DOI: 10.1109/TUFFC.2018.2881727.

[8] A. Ozgurluk, K. Peleaux and C. T.-C. Nguyen, "Single-Digit-Nanometer Capacitive-Gap Transduced Micromechanical Disk Resonators," in *IEEE 33rd International Conference on Micro Electro Mechanical Systems (MEMS)*, Vancouver, BC, Canada, Jan. 2020, pp. 222-225.

[9] M. Akgul, B. Kim, Z. Ren and C. T.-C. Nguyen, "Capacitively transduced micromechanical resonators with simultaneous low motional resistance and Q>70,000," in *Solid-State Sensor, Actuator, and Microsystems Workshop*, Hilton Head, South Carolina, USA, June 2010, pp. 467-470.

[10] D. Griffith, E. T.-T. Yen, P. T. R∅ine, K. Tsai and B. Goodlin, "A crystal-less bluetooth low energy radio using a MEMS-based frequency reference system," in *2017 Joint Conference of the European Frequency and Time Forum and IEEE International Frequency Control Symposium (EFTF/IFCS)*, Besancon, France, July 2017, pp. 181-184.

[11] A. Kourani, R. Lu, A. Gao and S. Gong, "A 300-500 MHz Tunable Oscillator Exploiting Ten Overtones in Single Lithium Niobate Resonator," in *Joint Conference of the IEEE International Frequency Control Symposium and European Frequency and Time Forum (EFTF/IFC)*, Orlando, FL, USA, April 2019, pp. 1-4.

[12] J. Stegner, U. Stehr, C. Tu, J. E.-Y. Lee and M. A. Hein, "Very-low phase noise RF-MEMS reference oscillator using AlN-on-Si resonators achieved by accurate co-simulation," in *IEEE MTT-S International Microwave Symposium (IMS)*, Honololu, HI, USA, June 2017, pp. 1303-1306.

[13] A. Ozgurluk, K. Peleaux and C. T.-C. Nguyen, "Widely tunable 20-nm-gap ruthenium metal square-plate resonator," in *Tech. Dig. 32nd IEEE Int. Conf. on Micro Electro Mechanical Systems (MEMS)*, Seoul, South Korea, Jan. 2019, pp. 153-156.